

AD-A265 900



2

OFFICE OF NAVAL RESEARCH

Contract No. N00014-91-J-1409

Technical Report No. 141

Electrode Potential-Induced Reconstruction of Au(100):

Effect of Chemisorption on Nanoscale Dynamics

as Probed by In-Situ Scanning Tunneling Microscopy

by

Xiaoping Gao and Michael J. Weaver

Prepared for Publication

in

Journal of Physical Chemistry

Department of Chemistry

Purdue University

West Lafayette, IN 47907-1393


April 1993

DTIC  
ELECTE  
JUN 17 1993  
S E D

Reproduction in whole, or in part, is permitted for any purpose of the United States Government.

\* This document has been approved for public release and sale; its distribution is unlimited.

93 6 16 080

93-13651  


Abstract

The effect of iodide chemisorption on the nanoscale real-space dynamics associated with the electrode potential-induced formation and removal of the hexagonal reconstruction on Au(100) in aqueous solution has been examined by means of in-situ scanning tunneling microscopy under potentiodynamic conditions. Unlike in "non-adsorbing" media such as perchloric acid where the  $(1 \times 1) \rightarrow (\text{hex})$  phase change is slow ( $t_{1/2} \sim 10$  min), requiring adatom diffusion from terrace edges, the potential-induced transition in iodide can be remarkably rapid ( $< 0.2$  s). The latter features facile large-scale (ca 10-20 nm) gold mass transport emanating from former  $(1 \times 1)$  terraces as well as from terrace edges. The likely roles of chemisorption in inducing such remarkably rapid reconstruction are briefly discussed.

Accession For	
NTIS CRA&I	<input checked="" type="checkbox"/>
DTIC TAB	<input type="checkbox"/>
Unannounced	<input type="checkbox"/>
Justification .....	
By .....	
Distribution /	
Availability Codes	
Dist	Avail and/or Special
A-1	

DTIC QUALITY INSPECTED 2

The phenomenon of metal surface reconstruction, whereby the top atomic layer assumes ordered structures that can differ markedly from the bulk-phase crystal lattice, is a well-studied (albeit inadequately understood) topic in vacuum surface science.<sup>1</sup> Reconstruction is also anticipated to occur on ordered surfaces in electrochemical environments. While broadbased data are lacking, some interesting information has been obtained recently for low-index gold surfaces in aqueous media.<sup>2</sup> Intriguingly, these surfaces exhibit stable reconstructed phases similar to that observed for the corresponding metal-vacuum interface only at negative (or near-zero) electronic charge densities, the reconstruction being lifted at more positive charges. Evidence for such charge- (or potential-) dependent reconstruction was obtained originally from electrochemical<sup>3</sup> and in-situ spectroscopic measurements.<sup>4</sup> However, the recent emergence of grazing incidence X-ray scattering (GIXS)<sup>5,6</sup> and scanning tunneling microscopy (STM)<sup>7-10</sup> are currently transforming our atomic-level structural understanding of these systems. These in-situ techniques are largely complementary: while GIXS usually provides more accurate atomic spatial information, STM can yield direct real space/time insight into the local (down to true atomic-level) structural changes associated with surface reconstruction.

Perhaps the most interesting system in this regard is Au(100). The square-planar (1 × 1) surface that is stable at positive electrode charges reverts to a hexagonal reconstructed phase at negative charges.<sup>5,7</sup> The latter, which forms a (5 × 27) unit cell on ideal terraces, also exhibits a myriad of local structural mutations as discerned by STM.<sup>7b</sup> The kinetics of the potential-induced (1 × 1) → (hex) phase transition are slow ( $t_{1/2}$  ~ 10 min) in weakly adsorbing electrolytes such as perchloric or sulfuric acids, although the reverse transition can be rapid under voltammetric conditions.<sup>7d,e,11</sup> A key requirement is the need to incur substantial mass transport of gold since the latter

structure has a 24% higher surface atomic density than the former. Detailed information on the nanoscale real-space dynamics of the  $(1 \times 1) \leftrightarrow (\text{hex})$  transition has recently been obtained by "potentiodynamic STM" measurements, whereby images are acquired *during* electrode-potential perturbations (sweeps or steps).<sup>7e</sup> These results highlight the importance of nucleation and gold adatom mass transport to the hex phase growth in the absence of electrolyte specific adsorption.

Quite a different situation might be expected in the presence of strong electrolyte adsorption. A particularly interesting example is iodide, which is sufficiently strongly adsorbed on Au(100) and other gold surfaces to yield high and even near-saturated coverages below the polarizable potential limit in aqueous media. By analogy with the known effects of electron-donating adsorbates on surface reconstruction in vacuum,<sup>13</sup> it is therefore anticipated (and observed) that the Au(100) hex reconstruction will be lifted at substantially lower potentials in iodide electrolytes than in more weakly adsorbing media.

We present herein potentiodynamic STM data with the objective of unraveling the roles of iodide chemisorption on the nanoscale dynamical nature of the potential-dependent Au(100) reconstruction. In particular, the results demonstrate a remarkable influence of the adsorbed iodide on the gold surface mass transport associated with the  $(1 \times 1) \leftrightarrow (\text{hex})$  transition.

The experimental STM procedures are largely as described elsewhere.<sup>7,8</sup> The microscope is a Nanoscope II (Digital Instruments) with a bipotentiostat for *in-situ* electrochemical STM. The STM tips were tungsten wire etched electrochemically in 0.1 M KOH and insulated either with clear nail varnish or a thermosetting polyethylene plastic.<sup>7e</sup> Most STM images were obtained in the so-called "height mode" (i.e. at constant current). The Au(100) (hemisphere, 5 mm diameter) was prepared at CNRS, Meudon, France by Dr. A. Hamelin. It was

pretreated by flame annealing, and cooled partly in air and in ultrapure water immediately before transfer to the STM cell. The counter electrode was a gold wire. The quasi-reference electrode was a platinum wire for the iodide electrolytes, and an electrooxidized gold wire in the perchloric acid medium. All electrode potentials quoted here, however, are converted to the saturated calomel electrode (SCE) scale.

Figure 1 shows a typical cyclic voltammogram obtained at a slow sweep rate ( $5 \text{ mV s}^{-1}$ ) for ordered Au(100) in  $0.095 \text{ M NaClO}_4 + 5 \text{ mM NaI}$ . The voltammetric features seen over the cycled range  $-0.9 \text{ V}$  to  $0.1 \text{ V}$  vs SCE provide a clear signal that multiple potential-induced surface structural changes are taking place. All these features are reproducible upon repeated potential cycling, and also appear at higher sweep rates (at least up to  $0.2 \text{ V s}^{-1}$ ). Detailed information on the microscopic nature of these transitions can be obtained from parallel (or simultaneous) potentiodynamic STM data. The sharp, largely reversible, current-potential ( $i$ - $E$ ) spikes located at  $E \geq -0.32 \text{ V}$  are associated with the formation of distinct ordered iodide adlayer structures. The nature of these adlayers on gold low-index surfaces will be detailed in a combined electrochemical-STM study to be reported elsewhere.<sup>14</sup> The significant voltammetric feature for the present purposes is the large-amplitude current peak, labelled  $C_p$ , centered at about  $-0.6 \text{ V}$  during the positive-going potential sweep, located on a wider  $i$ - $E$  wave which is partnered by a similarly broad but more pronounced  $i$ - $E$  wave seen during the negative-going sweep. The charge contained within  $C_p$ ,  $18\text{--}20 \mu\text{C cm}^{-2}$ , is largely independent of the sweep rate over the range  $5$  to  $100 \text{ mV s}^{-1}$ , although the peak tends to broaden and a secondary feature appears at slightly higher potentials towards faster scan rates.

Potentiodynamic STM data obtained under similar voltammetric conditions as in Fig. 1 confirm that the sharp current spike labelled  $C_p$  is indeed associated

with the lifting of the hex reconstruction which is stable at more negative potentials (below ca  $-0.7$  V). (A related, yet smaller, voltammetric feature signaling the removal of reconstruction is also seen in weakly adsorbing electrolytes such as perchloric or sulfuric acid, but at much higher potentials,  $0.4-0.6$  V.<sup>7d,e,11</sup>) The reconstruction is also seen to be reformed entirely by about  $-0.7$  V during the negative-going sweep under these conditions ( $5 \text{ mV s}^{-1}$ ). The "reversible potential" for the (hex)  $\leftrightarrow$  ( $1 \times 1$ ) interconversion,  $E_{\text{rec}}$ , in iodide is therefore substantially lower (i.e. more negative) than the value, ca  $0.3-0.4$  V, obtained in perchloric acid.<sup>7e</sup> Interestingly, back-integration of differential capacitance-potential data<sup>14</sup> shows that in both cases  $E_{\text{rec}}$  is situated slightly positive of the potential of zero charge,  $E_{\text{pzc}}$ , for the hex surface.<sup>15</sup> This point necessarily corresponds to the maximum in the surface tension-potential ( $\gamma - E$ ) curve, close to where the (hex)  $\leftrightarrow$  ( $1 \times 1$ ) phase transition would be anticipated.<sup>7e,15</sup> Physically, the marked ( $0.7$  V) shift in  $E_{\text{pzc}}$  between perchlorate and iodide electrolytes arises from the substantial iodide coverage,  $\theta_{\text{I}} \sim 0.15$ , formed by this point,<sup>14</sup> triggering the stabilization of the ( $1 \times 1$ ) substrate configuration.

Given the rapidity of the Au(100) reconstruction dynamics in aqueous iodide, it is advantageous to present here potentiodynamic STM data gathered during appropriate potential-step, rather than -sweep, excursions. Figures 2A-F show a temporal sequence of large-area (ca  $100 \times 100$  nm) STM images obtained for Au(100) in  $10 \text{ mM}$  KI during periodic potential steps from about  $-0.75$  to  $-0.45$  V; i.e. from either side of the potential region where the (hex)  $\leftrightarrow$  ( $1 \times 1$ ) interconversion is observed on the voltammetric timescale. The first image, A, was acquired shortly (within 1 min) after stepping to  $-0.75$  V. A uniform, essentially complete, hex reconstruction is seen throughout the imaged area, including the regions on either side of the terrace edge running through the

left-middle portion. The presence of the hex reconstruction is readily identified even on these large-scale images from the parallel corrugations which run roughly parallel to the substrate atomic rows, each spaced five gold atomic diameters (14.5 Å) apart. (As described in detail elsewhere, these z-corrugations arise from the periodic alterations in binding site geometry of the near-hexagonal reconstructed gold top layer on the underlying square-planar substrate.<sup>7b</sup>) Another interesting feature in Fig. 2A is the darker regions, thereby identified as "pits", prevalent on the largest terrace, which are uniformly one atomic-layer deep. These cavities were formed immediately along with the reconstruction. Close inspection of the pits themselves reveals the presence of the hex reconstruction uniformly across the crater floor.

Figure 2B, taken immediately after A, shows the effect of stepping the potential to -0.45 V. This perturbation was applied while the tip was being rastered downwards, about one-third down the imaged area. Inspection of Fig. 2B shows that the reconstruction is immediately ( $< 0.2$  s) and completely lifted at this point. Figure 2C is a close up of a portion of Fig. 2B, showing more clearly the discontinuous fashion in which the reconstruction is removed. Furthermore, the terrace edge running diagonally from the top left corner in Fig. 2B has shifted immediately towards the left (by ca 50-100 Å), and large one-atom high mesas now populate the terraces. Evidently, then, the additional surface gold atoms released upon lifting the reconstruction can collectively be transported rapidly over substantial distances under these conditions. The following STM image, Fig. 2D, obtained immediately thereafter (by rastering the tip upward) while holding the electrode potential at -0.45 V, shows that significant "surface annealing" has taken place, even on this short timescale. (Note that each image is acquired over ca 20 s.) Thus the smaller mesas observed in B have now disappeared, and the terrace edge referred to above has become

straighter and progressed further to the left.

Figure 2E shows the effect of stepping the potential back to  $-0.75$  V, again after the tip has been rastered about one-third down the imaged area. Similarly to the positive-going potential step, abrupt structural changes are seen, now acting to reform immediately the hex reconstruction. The required atoms are in part taken from the formerly  $(1 \times 1)$  terrace, as evidenced clearly by the immediate formation of the pits noted in Fig. 2A. For regions closer to terrace edge, however, pits are not formed, the additional atoms required being taken instead from the terrace edge which thereby undergoes marked erosion. Note that the hex corrugations tend to run parallel to the terrace edge in these circumstances, consistent with the mass transport of metal atoms required to increase the atomic density normal to the corrugation direction. The image F, acquired immediately after E while holding the potential at  $-0.75$  V, again shows an interesting structural evolution. In particular, the pits have undergone some aggregation and the major hex reconstruction domain, running roughly parallel to the terrace edge noted above, has spread to encompass a large fraction of the terrace.

Figure 3 is a typical "constant height" image for a Au(100) surface region in  $10$  mM KI, formerly consisting of a large uniform  $(1 \times 1)$  terrace created by holding the potential at ca  $-0.4$  V; the image was obtained upon sweeping the potential to  $-0.75$  V so to yield a hex reconstructed surface. The monoatomic deep pits appearing along with the reconstruction are seen to occupy about 20% of the imaged area. This observation is consistent with the additional 24% of the surface gold atoms required to form the hex reconstruction being wrested chiefly from the terrace itself.

It is interesting to compare these potential-induced structural changes with the  $(1 \times 1) \rightarrow$  (hex) conversion dynamics observed in the absence of specific



anion adsorption. The latter condition will be discussed in some detail elsewhere,<sup>7e</sup> so that only a brief description is provided here. Figures 4A-D are a representative sequence of large area (100 × 100 nm) images obtained in an electrolyte, 0.1 M HClO<sub>4</sub>, that exhibits little or no specific adsorption under the relevant conditions. The first image, A, shows a pair of adjacent (1 × 1) terraces formed by holding the potential at 0.4 V for 15 min, whereupon any hex domains present are removed. The small (ca 5 nm diameter) "brighter" regions are again monoatomic mesas formed from the excess gold atoms. (A larger density of such mesas can be formed when the (hex) → (1 × 1) conversion is driven to occur more rapidly, such as during positive-going potential sweeps.)<sup>7d,e</sup> Stepping the potential to markedly lower values, ca -0.3 V, yields a slow yet progressive formation of hex surface domains. Image B, taken about 1 min after the potential step, shows that a number of thin "strings" have appeared, running approximately along both (1 × 1) gold atomic directions (90° to each other), but preferentially formed parallel to the terrace edge. As detailed elsewhere,<sup>7b,e</sup> these strings consist of at least one additional gold atomic row imbedded in the otherwise (1 × 1) terrace and packing hexagonally with the immediately surrounding substrate atoms. These long hex "microdomains" grow both in density and breadth with time, as illustrated in C and D, recorded about 1 and 7 min, respectively, after B. Eventually, after 15-20 min, the hex domains cover a large (> 50%) fraction of the surface.

The likely microscopic mechanisms responsible for hex domain growth under these conditions are discussed in ref. 7e. Briefly, the mesas clearly provide an initially important source of the ca 24% additional gold atoms required to form the (5 × 27) from the (1 × 1) substrate. Figure 4 shows clearly how longer terrace edges can also act as quarries for the atoms required, as adjudged from the marked straightening and alignment with the hex strings seen as the

reconstruction develops. Nevertheless, the numerous additional strings seen to form at longer times within flat terrace regions already surrounded entirely by the other hex domains (see Fig. 4C and D versus B, for example) indicate that some of the additional gold atoms arrive via longer-range surface diffusion.

Comparison of Figs. 2 and 4 exposes some dramatic differences in the morphology as well as rates of hex domain growth in the presence and absence of chemisorbed iodide. Most obviously, the formation as well as removal of the surface reconstruction in the presence of iodide features sudden (< few sec) large-scale (ca 10-50 nm) alterations in the terrace morphology. These changes occur only in a severely muted form and over a much larger (ca 10 min) timescale in the absence of chemisorption. The former transformations encompass large (ca 100 Å) shifts in the position as well as shape of terrace edges, and the formation or removal of monoatomic pits and mesas. In addition, the hex phase is seen to appear essentially *uniformly* within a given terrace region in the presence of iodide, rather than initially as narrow hex strands as seen in the absence of chemisorption.

These profound changes in the dynamics of the  $(1 \times 1) \rightarrow (\text{hex})$  transition can be rationalized in terms of the alterations in gold surface diffusion engendered by iodide chemisorption. In the absence of iodide, the surface diffusion required for propagating the reconstruction appears limited to gold *adatoms*, i.e. those not forming part of the  $(1 \times 1)$  terrace in an equilibrium sense. These adatoms are transported from terrace edges or mesas. In the presence of iodide chemisorption a significant or even large fraction of the terrace gold atoms become significantly mobile to contribute to the substantial and rapid surface mass flow which is seen to occur. This assertion is supported by the observed facile formation of monoatomic pits within large terraces when forming the hex phase in iodide. The initial distances between the pits, 5-10

nm, (produced within ca 5 s of the potential step) provides information on the long-range nature of the surface diffusion involved. Such pits are largely absent during hex formation in perchloric acid. In iodide, then, the additional surface atoms required for hex formation can be taken readily by disrupting the uniform (1 × 1) terrace, at least away from the terrace edges that provide the alternate source of atoms.

The formation of gold-iodide bonds (with the iodine atoms located preferentially in hollow binding sites<sup>12,14</sup>) should weaken the gold-gold bonding,<sup>18</sup> thereby facilitating x-y motion of the top-layer substrate atoms. Nonetheless, the formation of Au-I "surface complexes" featuring partial oxidation (and solvation) to form, say, Au<sup>I</sup>, seems unlikely given that gold surface dissolution (as AuI<sub>2</sub><sup>-</sup>) does not commence until a much higher potential, ca 0.6 V, than those (ca -0.6 V) where the hex → (1 × 1) transition takes place. Interestingly, the occurrence of chloride adsorption has been seen to enhance markedly the metal atom mobility on polycrystalline gold electrodes.<sup>19</sup> The presence of interfacial water is also known to facilitate mass flow on gold surfaces.<sup>20</sup>

Since large ordered terraces of either hex reconstructed or (1 × 1) structures may be formed merely by selecting the appropriate electrode potential in iodide media, the present results may have practical significance as a straightforward means of achieving "room-temperature surface annealing." A similar observation also holds for Au(110).<sup>14</sup> More fundamentally, the findings illustrate the intriguing degree of control on the atomic-level structure and dynamics of metal surfaces that can be achieved by appropriate adjustments in the chemical and electrical state within interfacial electrochemical environments, along with highlighting the virtues of in-situ STM for exploring such issues.

### Acknowledgments

We are grateful to Greg Edens for some electrochemical measurements, and to Antoinette Hamelin for supplying the gold crystal and for stimulating discussions. This work is supported by the Office of Naval Research and the National Science Foundation.

### References and Notes

- (1) For a review see: Van Hove, M.A., Wang, S-W., Ogletree, D.F., Somorjai, G.A., *Adv. Quantum Chem.*, 1989, 20, 1.
- (2) For recent overviews, see: (a) Kolb, D.M., in "Frontiers of Electrochemistry", Vol. 2, Lipkowsky, J., Ross, P.N., eds., VCH Publishers, New York, 1993; (b) Weaver, M.J., Gao, X., *Ann. Rev. Phys. Chem.*, in press.
- (3) Hamelin, A., *J. Electroanal. Chem.*, 1982, 142, 299.
- (4) Kolb, D.M., Schneider, J., *Surf. Sci.*, 1985, 162, 764.
- (5) (a) Ocko, B.M., Wang, J., Davenport, A., Isaacs, H., *Phys. Rev. Lett.*, 1990, 65, 1466; (b) Tidswell, I.M., Markovic, N.M., Lucas, C.A., Ross, P.N., *Phys. Rev. B.*, in press.
- (6) (a) Wang, J., Ocko, B.M., Davenport, A.J., Isaacs, H.S., *Phys. Rev. B*, 1992, 46, 10321; (b) Ocko, B.M., Helgensen, G., Schardt, B., Wang, J., Hamelin, A., *Phys. Rev. Lett.*, 1992, 69, 3350.
- (7) (a) Gao, X., Hamelin, A., Weaver, M.J., *Phys. Rev. Lett.*, 1991, 67, 618, (b) Gao, X., Hamelin, A., Weaver, M.J., *Phys. Rev. N*, 1992, 46, 7097; (c) Hamelin, A., Gao, X., Weaver, M.J., *J. Electroanal. Chem.*, 1992, 323, 361; (d) Hamelin, A., Stoicoviciu, L., Edens, G., Gao, X., Weaver, M.J., *J. Electroanal. Chem.*, submitted; (e) Gao, X., Edens, G., Hamelin, A., Weaver, M.J., *Surf. Sci.*, submitted.
- (8) (a) Gao, X., Hamelin, A., Weaver, M.J., *J. Chem. Phys.*, 1991, 95, 6993; (b) Gao, X., Hamelin, A., Weaver, M.J., *Phys. Rev. B*, 1991, 44, 10983; (c) Gao, X., Weaver, M.J., *Ber. Bunsenge. Phys. Chem.*, 1993, 97, 507.

- (9) Tao, N.J., Lindsay, S.M., *J. Appl. Phys.*, 1991, 70, 5141; (b) Tao, N.J., Lindsay, S.M., *Surf. Sci.*, 1992, 274, L546.
- (10) Kolb, D.M., et al, submitted to *Surf. Sci.*
- (11) Schneider, J., Kolb, D.M., *Surf. Sci.*, 1988, 193, 579.
- (12) Gao, X., Weaver, M.J., *J. Am. Chem. Soc.*, 1992, 114, 8544.
- (13) Somorjai, G.A., Van Hove, M.A., *Prog. Surf. Sci.*, 1989, 30, 201.
- (14) Gao, X., Edens, G., Weaver, M.J., in preparation.
- (15) Since iodide adsorption involves near-complete adsorbate-surface charge transfer on gold,<sup>12</sup> the "formal"  $E_{pzc}$  value extracted by presuming that iodide retains its ionic charge upon adsorption ("ideally polarizable" assumption) will differ from the actual  $E_{pzc}$  value which accounts for such charge sharing. Nonetheless, the former  $E_{pzc}$  value will always correspond to the maximum in the surface tension-potential (electrocapillary) curve,<sup>16</sup> upon which the potential-dependent thermodynamics of the hex  $\rightarrow$  (1  $\times$  1) surface phase transition should inherently depend.<sup>7e,17</sup>
- (16) Frumkin, A.N., Petri, O.A., Damaskin, B.B., in "Comprehensive Treatise of Electrochemistry", Vol. 1, Bockris, J. O'M., Conway, B.E., Yeager, E., eds., Plenum Press, New York, 1980.
- (17) Ross, P.N., D'Agostino, A.T., *Electrochim. Acta*, 1992, 37, 615.
- (18) Sette, F., Hashizume, T., Comin, F., MacDowell, A.A., Citrin, P.H., *Phys. Rev. Lett.*, 1988, 61, 1384.
- (19) (a) Garcia, M.P., Gómez, M.M., Salvarezza, R.C., Arvia, A.J., *J. Electroanal. Chem.*, 1993, 347, 237; (b) Doña, J.M., González-Velasco, J., *Surf. Sci.*, 1992, 274, 205.
- (20) Peale, D.R., Cooper, B.H., *J. Vac. Sci. Technol.*, 1992, A10, 2210.

### Figure Captions

#### Figure 1

Cyclic voltammogram at  $5 \text{ mV s}^{-1}$  for Au(100) in  $0.095 \text{ M NaClO}_4 + 5 \text{ mM NaI}$ .

#### Figure 2

Sequence of large-area STM images for Au(100) in  $10 \text{ mM KI}$  during potential-induced (hex)  $\leftrightarrow$   $(1 \times 1)$  phase transition. Acquisition time of each image (upward- or downward-rastered) is 20 s. A) At  $-0.75 \text{ V vs SCE}$ . B) Downward-rastered image with potential step from  $-0.75 \text{ V}$  to  $-0.45 \text{ V}$ , showing immediate removal of reconstruction. C) Close up of a portion of B. D) Upward-rastered image at  $-0.45 \text{ V}$  acquired immediately after B. E) Downward-rastered image with step from  $-0.45 \text{ V}$  to  $-0.75 \text{ V}$ , showing sudden reformation of reconstruction. F) Image at  $-0.75 \text{ V}$ , acquired immediately after E.

#### Figure 3

"Constant-height" STM image for Au(100) terrace region in  $10 \text{ mM KI}$ , obtained after sweeping potential from  $-0.4$  to  $-0.75 \text{ V}$  so to yield uniform reconstruction (see text).

#### Figure 4

Sequence of large-area STM images for Au(100) during slow formation of hex reconstruction at  $-0.3 \text{ V}$  in  $0.1 \text{ M HClO}_4$ . A) Pair of  $(1 \times 1)$  terraces formed by holding potential at  $0.4 \text{ V}$  for 15 min. B) 1 min after stepping potential from  $0.4$  to  $-0.3 \text{ V}$ . C) 1 min after B. D) 7 min after B.

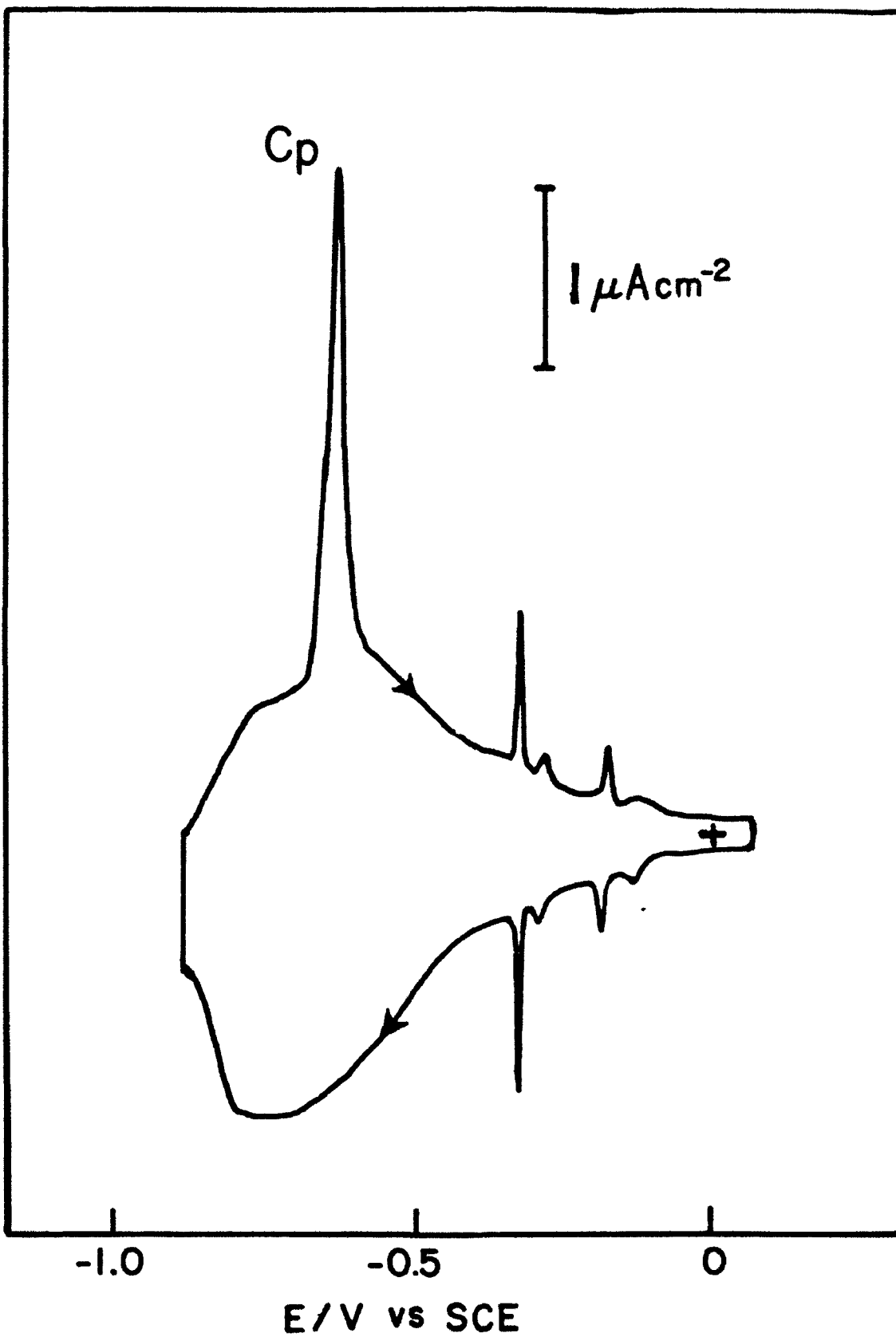
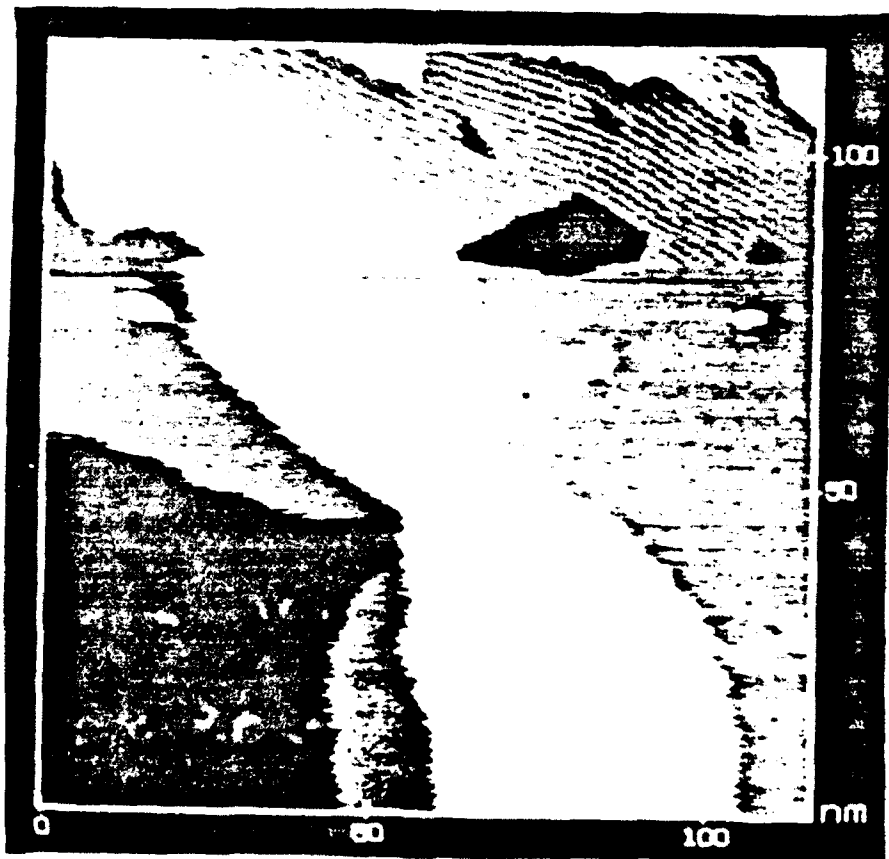


FIG 1



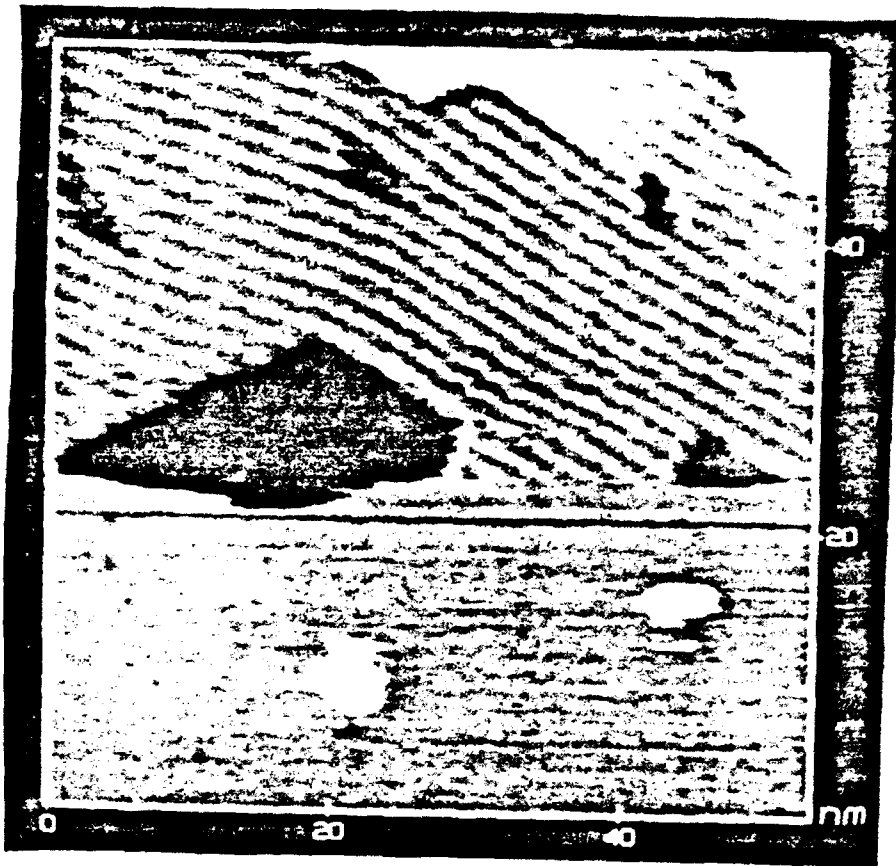
A



B

FIG 2





C

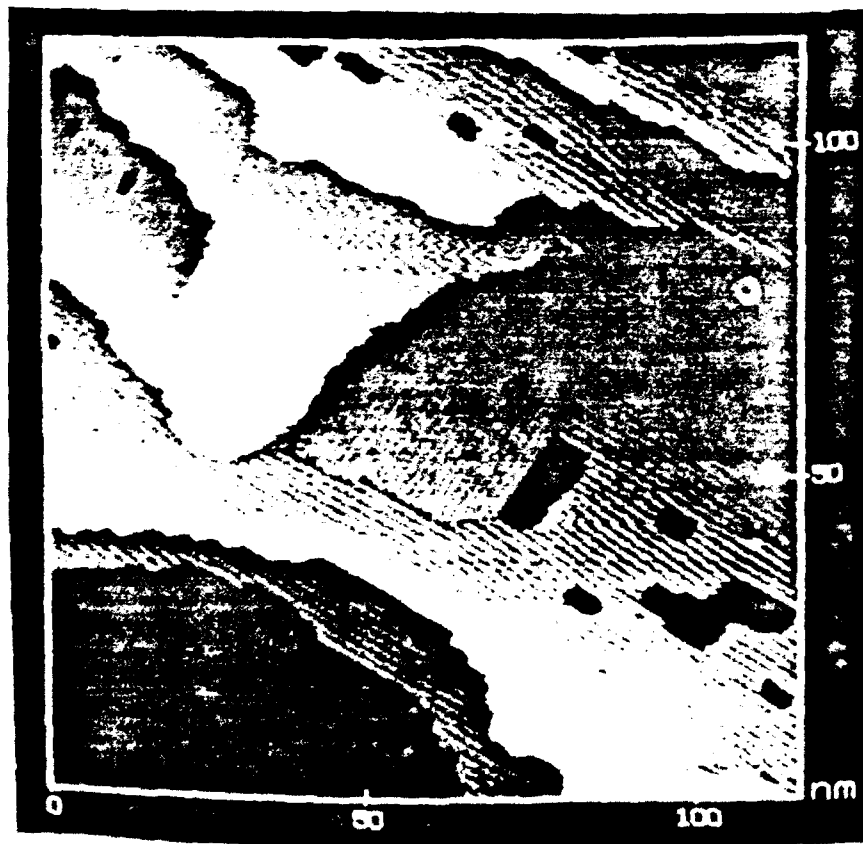


D

FIG 2 (contd)



E



F

FIG 2 (CONT'D)

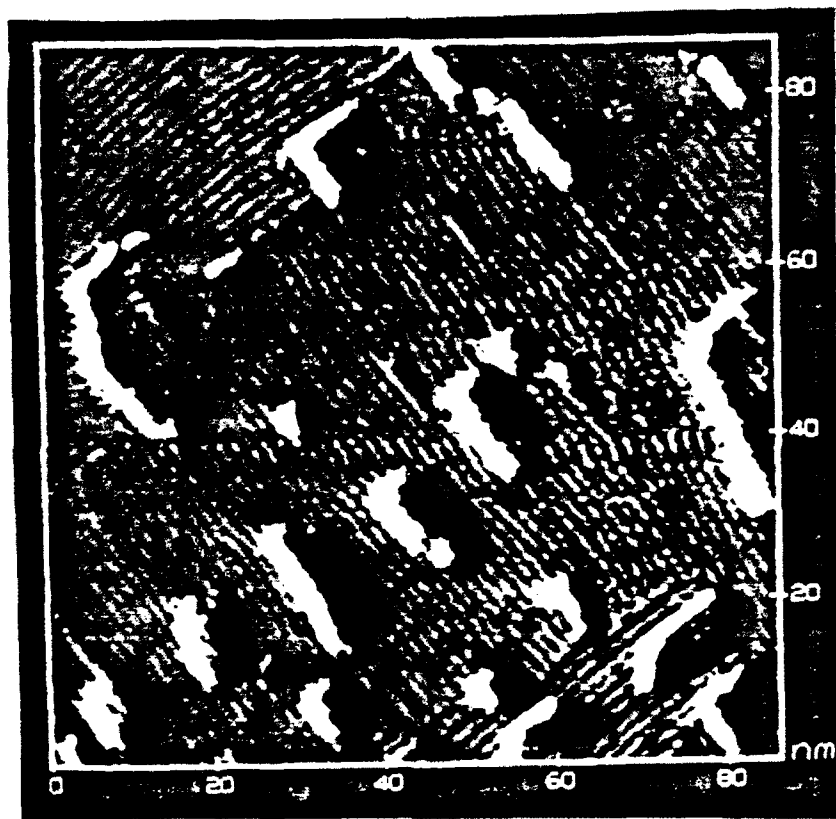
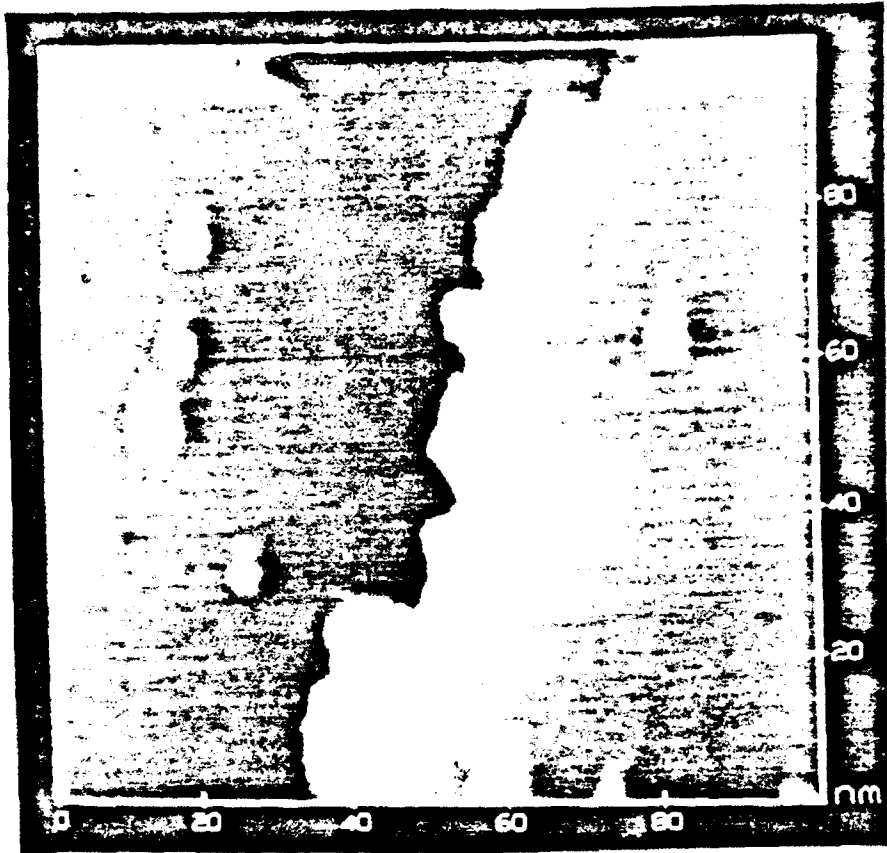
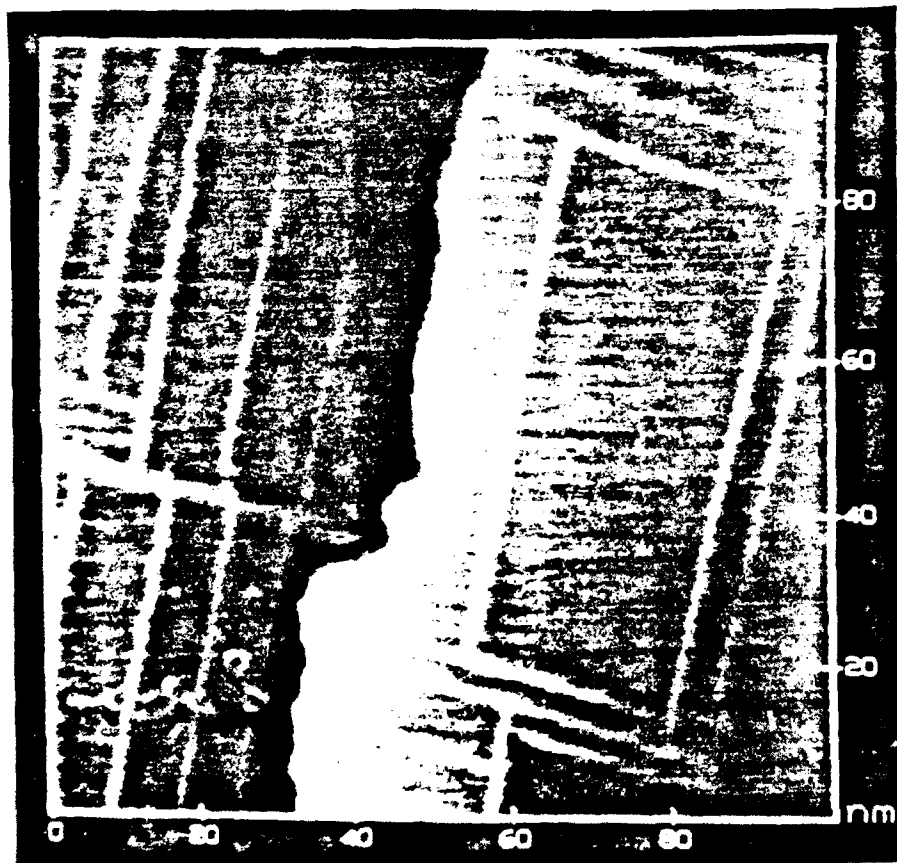


FIG 3



A



B

FIG 4



C



D

FIG 4 (CONT'D)